ISSN 1063-7788, Physics of Atomic Nuclei, 2008, Vol. 71, No. 3, pp. 493–508. © Pleiades Publishing, Ltd., 2008.
Original Russian Text © B.S. Ishkhanov, V.N. Orlin, 2008, published in Yadernaya Fizika, 2008, Vol. 71, No. 3, pp. 517–531.

NUCLEI
Theory

Preequilibrium Model of Photonucleon Reactions That Is Based on Fermi Gas Densities

B. S. Ishkhanov and V. N. Orlin

Institute of Nuclear Physics, Moscow State University, Vorob'evy gory, Moscow, 119992 Russia

Received April 20, 2007; in final form, August 27, 2007

Abstract—A combination of the exciton and evaporation models is used to describe photonucleon reactions induced in heavy and medium-mass nuclei by photons of energy in the range $7 \leq E_\gamma \leq 140$ MeV. The formation of a giant dipole resonance and quasideuteron absorption are considered as two mechanisms that are responsible for the photoexcitation of a nucleus in the energy regions $E_\gamma \lesssim 20$ MeV and $E_\gamma \gtrsim 40$ MeV, respectively. As is well known, the densities of particle–hole states are employed in the exciton model, and these quantities are calculated on the basis of the Fermi gas model. This makes it possible to take into account the effect of the energy dependence of single-particle and single-hole densities of states on the rate of emission and intranuclear processes. The model in question is applied to describing partial photonucleon cross sections for ^{119}Sn, ^{140}Ce, ^{181}Ta, and ^{208}Pb nuclei.

PACS numbers: 25.20.-x
DOI: 10.1134/S1063778808030101

1. INTRODUCTION

In order to describe various photonucleon reactions occurring upon photon absorption by a nucleus, it is necessary (i) to know the cross section for the formation of the initial excited nucleus (photoabsorption cross section) and (ii) to consider all possible or at least the most important nucleon-emission processes caused by this excitation.

An electromagnetic field interacts with a nucleus predominantly through its $E1$ component. At low absorbed-photon energies ($E_\gamma \lesssim 20$ MeV), in which case the long-wavelength approximation is valid, this leads to the excitation of a giant dipole resonance (GDR), since self-sustained synchronous vibrations of all neutrons with respect to all protons arise under the effect of an external $E1$ field. With increasing photon energy, the photon wavelength decreases, with the result that the quasideuteron (QD) photoabsorption mechanism, which is different from the above GDR mechanism and according to which a dipole excitation is transferred to spatially correlated individual neutron–proton pairs [1–3] rather than to the entire nucleus as a discrete unit, becomes dominant (from $E_\gamma \gtrsim 40$ MeV up to the pion production threshold). Thus, the total photoabsorption cross section $\sigma_{\text{abs}}(E_\gamma)$ can be approximately represented as the sum of two terms; that is,

$$\sigma_{\text{abs}}(E_\gamma) = \sigma_{\text{GDR}}(E_\gamma) + \sigma_{\text{QD}}(E_\gamma), \quad (1)$$

where $\sigma_{\text{GDR}}(E_\gamma)$ is the cross section for GDR excitation and $\sigma_{\text{QD}}(E_\gamma)$ is the cross section for quasideuteron photoabsorption.

The cross section $\sigma_{\text{GDR}}(E_\gamma)$ can be calculated on the basis of the semimicroscopic giant-dipole-resonance model developed in [4–6]. This model makes it possible to describe satisfactorily the GDR strength function without resort to adjustable parameters (the quadrupole deformation of a nucleus, the only free parameter in the model, can be determined from data on static quadrupole momenta of nuclei [7]). For the quasideuteron component of the photoabsorption cross section, Levinger [1, 2] obtained a phenomenological expression, whose parameters were estimated in [3] on the basis of the Fermi gas model.

The character of photonucleon emission depends greatly on the nature of the primary excitation of the nucleus involved. The GDR component of photonucleon reactions proceeding on heavy and medium-mass nuclei is determined primarily by nucleon emission from the compound nuclear state formed upon the thermalization of the energy of dipole vibrations. (For a first approximation, we can restrict our consideration to equilibrium neutron emission, since the Coulomb barrier strongly suppresses proton evaporation.) As for the effect of preequilibrium nucleon emission in GDR decay, it is comparatively small, manifesting itself primarily in the region of the giant-resonance maximum ($E_\gamma \lesssim 20$ MeV), where there occurs the formation of a coherent *single-particle—single-hole* ($1p1h$) doorway state.

On the other hand, preequilibrium nucleon emission has a significant effect on the quasideuteron component of photonucleon reactions, since, in the case of quasideuteron photoabsorption, the entire energy of a hard photon is transferred to a single neutron—proton pair. This circumstance was demonstrated in the analyses performed in [8] and [9] within semiclassical preequilibrium models (exciton model [10—13] and hybrid model [14—16], respectively) and in the later study of Chadwick and Young [17], who described preequilibrium processes on the basis of the multistep quantum-mechanical model developed by Feshbach, Kerman, and Koonin [18].

In semiclassical preequilibrium models dating back to the study of Griffin [19], it is assumed that, at any stage of the reaction being considered, the state of the nuclear system involved can be characterized by the excitation energy E, the number of excited particles (p), and the number of holes (h). It is also assumed that all possible ph configurations characterized by the same exciton number $m = p + h$ are populated with equal probabilities. The evolution of the nuclear system starts from a simple doorway state featuring a small number of particles and holes, $m_0 = p_0 + h_0$. This state either emits a nucleon into the continuous spectrum or undergoes a transition to one of the $(m_0 + 2)$ exciton states because of nucleon—nucleus collisions leading to the formation of yet another particle—hole pair. After that, this step is repeated. The $(m_0 + 2)$ exciton state formed in this way either emits a nucleon into a continuous spectrum or undergoes the $m_0 + 2 \to m_0 + 4$ intranuclear transition and so on. The cascade of $m_0 \to m_0 + 2 \to m_0 + 4 \to \ldots$ intranuclear transitions is accompanied by the redistribution of the excitation energy of the nucleus among an ever increasing number of particles and holes. At the same time, the $\ldots \to m_0 + 4 \to m_0 + 2 \to m_0$ inverse transitions may occur owing to the annihilation of one of the pairs via the transfer of its energy to some particle or some hole. The role of such transitions is insignificant as long as the total number of particles and holes in the system is moderate. As this number increases, however, the probability of the transitions in question grows gradually, ultimately becoming equal to the probability of direct transitions. At this instant, the system reaches a state of thermal equilibrium. However, preequilibrium nucleon emission ceases to occur long before equilibration (at the first reaction stages); therefore, one often disregards inverse transitions in describing an intranuclear cascade.

In semiclassical preequilibrium models, the probability per unit time of the process in which the decay of the m-exciton state is accompanied by the emission of a nucleon into the continuous spectrum is determined on the basis of statistical concepts by using the detailed-balance principle, but this leads to some loss of information, especially in describing angular distribution of reaction products. In view of this, more sophisticated quantum-mechanical preequilibrium-decay models [18, 20—25], in which the rate of nucleon emission is determined in terms of quantum-mechanical transition amplitudes, have been vigorously developed in recent years. Nevertheless, the drawbacks of semiclassical models are counterbalanced to a considerable extent by the fact that they are quite simple in applications and possess a high predictive power. Owing to this, they have so far been widely used in specific calculations [26, 27].

Among a wide variety of semiclassical preequilibrium models, the exciton model [10—13] and the hybrid model [14—16] have become the most popular. These models differ primarily in how the process of intranuclear transitions between various intermediate states of the nuclear system is described in them. While, in the exciton model, one estimates the average rate of the transition from the m-exciton to the $(m + 2)$-exciton configuration (this being fully consistent with the assumption that all ph states belonging to the same $\{E, m\}$ class are populated with equal probabilities), in the hybrid model, one calculates an individual transition rate for each ph configuration, this invalidating the use of the hypothesis of equiprobable populations of ph states at later reaction stages. This inconsistency inherent in the hybrid model was highlighted in [28], where the degree of mixing of configurations that belong to the same exciton class was estimated within the exciton and hybrid models. Ten years after that, Blann [29] and Blann and Chadwick [30] removed this inconsistency, proposing an alternative approach that they referred to as a hybrid Monte Carlo (HMK) simulation. This approach is conceptually consistent, but it leads to much more cumbersome calculations than simple semiclassical models. This is the reason why, even at the present time, the self-consistent exciton model provides a good choice for performing semiclassical calculations of preequilibrium processes.[1)]

[1)]The exciton model was recently criticized by Soares Pompeia and Carlson [31], who compared the results obtained by describing nucleon—nucleus reactions on the basis of a Monte Carlo simulation (similar to that in the HMC approach) and on the basis of the exciton model and arrived at the conclusion that the hypothesis of the equiprobable population of ph states at each reaction stage is unjustified. However, this conclusion was not substantiated very well, since, in describing nucleon—nucleus reactions, those authors incorrectly chose the doorway state—$1p1h$ (in the simulation, the hole being at the Fermi surface) instead of $2p1h$—and this could not fail to affect the results of the comparison in question.

The use of ph densities that are based on an equidistant distribution of single-particle energy levels is a feature peculiar to generally accepted preequilibrium models [13, 23, 33]. This approximation makes it possible to simplify relevant calculations significantly, since analytic expressions were obtained for equidistant distributions; at the same time, its use leads to underestimating the fraction of high-energy particles in intermediate ph states, since, in fact, the density of single-particle nuclear levels grows with energy.

In the present study, we formulate an exciton-model version in which Fermi gas densities of ph states are used in describing preequilibrium processes. This choice of densities correlates with Chadwick's method [3] for estimating the parameters of the quasideuteron photoabsorpion model, on one hand, and makes it possible to take into account the effect of the energy dependence of the densities of single-particle and single-hole states on the dynamics of the development of the preequilibrium cascade, on the other hand. According to the Fermi gas model, the density of single-particle states grows with increasing excitation energy of particles; on the contrary, the density of single-hole states decreases to zero as the hole energy tends to its maximum value equal to the Fermi energy of about 35 MeV. It follows that, upon going over from the densities of equidistant levels to Fermi gas densities, which are more realistic, the fraction of high-energy particles increases at each step of the preequilibrium process, with the result that the relative role of primary preequilibrium emission becomes much more important. It is well known that, in existing models, multiparticle preequilibrium emission affects most strongly the description of partial photonucleon cross sections: the emission of a second fast particle reduces sharply the yield of subsequent final-state nuclei (having a smaller mass number A) [16, 34]. If one employs Fermi gas densities, this effect becomes weaker, since the energy carried away by the first emitted particle increases. Taking this circumstance into consideration, we decided to restrict ourselves here to the inclusion of primary preequilibrium emission. The details of the proposed model are discussed in Section 2. This model is used here to calculate the partial cross sections for photonucleon reactions on ^{119}Sn, ^{140}Ce, ^{181}Ta, and ^{208}Pb nuclei in the energy range $7 \leq E_\gamma \leq 140$ MeV. In Section 3, the results of these calculations are compared with experimental data from [35], which were obtained for targets of natural isotopic composition.

2. DESCRIPTION OF THE MODEL

2.1. Basic Relations

According to Bohr's hypothesis, a nuclear reaction can be broken down into two independent stages: the formation of a compound system and its decay to reaction products. Following this hypothesis, we represent the cross sections for (γ, kn) and $(\gamma, 1pln)$ reactions involving the emission of, respectively, k neutrons and one proton plus l neutrons as

$$\sigma(\gamma, kn; E_\gamma) \tag{2}$$

$$= \sigma_{\mathrm{GDR}}(E_\gamma)(1 - F(E_\gamma))W(kn, E_\gamma)$$

$$+ \delta_{k1}\sigma_{\mathrm{GDR}}(E_\gamma)F(E_\gamma) + \sigma_{\mathrm{QD}}(E_\gamma)P(kn, E_\gamma),$$

and as

$$\sigma(\gamma, 1pln; E_\gamma) = \sigma_{\mathrm{QD}}(E_\gamma)P(1pln, E_\gamma), \tag{3}$$

where E_γ is the absorbed-photon energy (excitation energy of the target nucleus), $\sigma_{\mathrm{GDR}}(E_\gamma)$ is the cross section for GDR excitation, $\sigma_{\mathrm{QD}}(E_\gamma)$ is the cross section for quasideuteron photoabsorption, $W(kn, E_\gamma)$ is the probability for the evaporation of k neutrons from the compound state of the target nucleus, $P(kn, E_\gamma)$ is the probability of quasideuteron-excitation decay accompanied by the emission of k neutrons that may include one preequilibrium neutron ($k = 1, 2, \ldots$), $P(1pln, E_\gamma)$ is the probability for the processes in which the decay of such a state is accompanied by the emission of one preequilibrium proton and l preequilibrium neutrons ($l = 0, 1, \ldots$), $F(E_\gamma)$ is the total probability of preequilibrium GDR decay at an energy of E_γ, and δ_{k1} is a Kronecker delta.

The first and second terms on the right-side of relation (2) describe, respectively, equilibrium and preequilibrium emission of neutrons from a giant dipole resonance. It is assumed here that preequilibrium GDR decay is due primarily to the emission of one preequilibrium neutron. The evaporation of protons is disregarded.

2.1.1. Probabilities $W(kn, E)$. In order to calculate the probabilities $W(kn, E)$ (where E is the excitation energy of the nucleus involved and $k = 1, 2, \ldots$), we make use of Weisskopf's evaporation model [36], which takes into account only energy conservation. According to this model, the energy spectrum $I(\varepsilon)$ of neutrons evaporated from the nucleus can be approximated by the Maxwellian distribution

$$I(\varepsilon) \approx \Theta^{-2}\varepsilon \exp\left[-\frac{\varepsilon}{\Theta}\right], \tag{4}$$

where ε is the emitted-neutron energy and Θ is the temperature of the final-state nucleus (in energy units) in the state of maximum excitation energy $\hat{U}$,

$$\Theta = \left(\frac{d\ln w}{dE}\right)^{-1}_{E=\hat{U}} = \frac{\sqrt{\hat{U}/a}}{(1-2/\sqrt{a\hat{U}})}. \quad (5)$$

Here, $\hat{U} = E - B_n$, B_n being the neutron-separation energy; $w(E) \propto E^{-2}e^{2\sqrt{aE}}$ is the nuclear-level density; and a is the level-density parameter.

The distribution in (4) satisfies the normalization condition $\int_0^{\hat{U}} I(\varepsilon)d\varepsilon \approx 1$ if the inequality $\hat{U} \gg \Theta$ holds, as it does indeed do in the following. The probability function $W(kn, E)$ can be represented in the form

$$W(kn, E) = Q(kn, E) - Q((k+1)n, E), \quad (6)$$

where the probability of the evaporation of not less than k neutrons is

$$Q(kn, E) \approx \int\limits_0^{E-B_{kn}} \varepsilon_1 \exp\left[-\frac{\varepsilon_1}{\Theta_1}\right]\Theta_2^{-2} \quad (7)$$

$$\times \int\limits_0^{E-B_{kn}-\varepsilon_1} \varepsilon_2 \exp\left[-\frac{\varepsilon_2}{\Theta_2}\right]\ldots\Theta_{k-1}^{-2}$$

$$\times \int\limits_0^{E-B_{kn}-\varepsilon_1-\ldots-\varepsilon_{k-2}} \varepsilon_{k-1} \exp\left[-\frac{\varepsilon_{k-1}}{\Theta_{k-1}}\right]d\varepsilon_1\ldots d\varepsilon_{k-1}$$

for $E \geq B_{kn}$ and is zero for $E < B_{kn}$. Here, B_{kn} is the energy of separation of k neutrons ($B_{1n} \equiv B_n$), $\Theta_i = \sqrt{\hat{U}_i/a}\left(1-2/\sqrt{a\hat{U}_i}\right)^{-1}$ is the maximum temperature, and $\hat{U}_i = E - B_{in} - \varepsilon_1 - \ldots - \varepsilon_{i-1} \geq B_{kn} - B_{in}$ is the maximum excitation energy of the ith intermediate nucleus ($i = 1, 2, \ldots, k-1$).

The integral in (7) can readily be calculated by using the approximation

$$\hat{U}_1 = E - B_{1n}, \quad (8)$$

$$\hat{U}_2 \approx \max(E - B_{2n} - \Theta_1, B_{kn} - B_{2n}), \ldots,$$

$$\hat{U}_{k-1} \approx \max(E - B_{kn} - \Theta_1 - \ldots - \Theta_{k-2},$$

$$B_{kn} - B_{(k-1)n}).$$

This assumes the approximation of the energies ε_1, $\varepsilon_2, \ldots, \varepsilon_{i-1}$ in the expression for $\hat{U}_i$ [see Eq. (7)] by their values at which one expects the maximum yield of primary, secondary, etc., neutrons [we note that the distribution in (4) attains a maximum at $\varepsilon = \Theta$].

2.1.2. Probabilities $P(kn, E)$ and $P(1pln, E)$. Quasideuteron absorption leads to the excitation of one neutron and one proton, generating a $2p2h$ doorway state (this nucleon configuration features $m = 4$ excitons). After that, the initial excited state decays either via the emission of an excited nucleon or (this is more probable) via an intranuclear transition to a more complex $3p3h$ configuration ($m = 6$), this transition being due to the residual two-body interaction. As the result of intranuclear ($m \to m+2$) transitions, the excitation energy of the compound system is redistributed between an ever increasing number of excitons until a state of thermal equilibrium is reached or until, at some m-exciton step, a nucleon is emitted into the continuum spectrum, whereupon the thermalization processes is completed in the residual nucleus. As soon as the compound state is reached (in the initial or in the residual nucleus), a rather long process of neutron evaporation begins. This is a simplified scheme of the evolution of the primary quasideuteron excitation. This scheme takes no account of inverse ($m \to m-2$) intranuclear transitions that are due to particle–hole recombination and whose probability is low or multiparticle preequilibrium emission, whose probability is greater at high excitation energies.

Following this scheme, we represent the probabilities of interest in the form

$$P(kn, E) = \sum_{\substack{m=4\\ \Delta m=2}}^{\bar{m}-2} \left[\frac{\int_0^{E-B_n} \lambda_n(m, \varepsilon, E) W_n((k-1)n, E - B_n - \varepsilon)d\varepsilon}{\Gamma^{\uparrow}(m, E)/\hbar + \Gamma^{\downarrow}(m, E)/\hbar}\right] D(m, E) + D(\bar{m}, E)W(kn, E), \quad (9)$$

$$P(1pln, E) = \sum_{\substack{m=4\\ \Delta m=2}}^{\bar{m}-2} \left[\frac{\int_0^{E-B_p} \lambda_p(m, \varepsilon, E) W_p(ln, E - B_p - \varepsilon)d\varepsilon}{\Gamma^{\uparrow}(m, E)/\hbar + \Gamma^{\downarrow}(m, E)/\hbar}\right] D(m, E). \quad (10)$$

Here, $k = 1, 2, \ldots$; $l = 0, 1, \ldots$; E is the excitation energy of the target nucleus; $\bar{m}$ is the average number of excitons in the state of thermal equilibrium; B_j is the separation energy for a nucleon of type j (a neutron, $j = n$, or a proton, $j = p$); $\lambda_j(m, \varepsilon, E)d\varepsilon$ is the probability per unit time for a process in which the decay of an m-exciton state is accompanied by the emission of a j-type nucleon of kinetic energy $\varepsilon \pm d\varepsilon/2$ into the continuous spectrum; $W_j(ln, U)$ is the probability of evaporation of l neutrons from the compound state of the residual nucleus, where $U = E - B_j - \varepsilon$ is the energy of this nucleus [for the calculation of $W_j(ln, U)$, see Subsection 2.1.1; $W_j(0n, U) = 1$ at U below the neutron-separation energy in the residual nucleus, and $W_j(0n, U) = 0$ in the opposite case]; $\Gamma^{\uparrow}(m, E)/\hbar$ is the total probability per unit time for the decay of an m-exciton state via nucleon emission [$\Gamma^{\uparrow}(m, E)$ is the emissive width of this state]; $\Gamma^{\downarrow}(m, E)/\hbar$ is the probability per unit time for an $m \to m + 2$ intranuclear transition via the production of yet another ph pair [$\Gamma^{\downarrow}(m, E)$ is the spreading width of an m-exciton state]; and, finally,

$$D(m, E) = \begin{cases} 1 & \text{for } m = 4, \\ \prod\limits_{\substack{n=4 \\ \Delta n = 2}}^{m-2} \dfrac{\Gamma^{\downarrow}(n, E)}{\Gamma^{\uparrow}(n, E) + \Gamma^{\downarrow}(n, E)} & \text{for } m = 6, 8, \ldots \end{cases} \tag{11}$$

is the probability that the chain of intranuclear transitions in the target nucleus reaches the m-exciton step.

From the detailed-balance principle, it follows that (see [10])

$$\lambda_j(m, \varepsilon, E)d\varepsilon \tag{12}$$

$$= \frac{2s + 1}{\pi^2 \hbar^3} \mu \varepsilon \sigma_j^{\text{inv}}(\varepsilon) \frac{\omega(m - 1, U)}{\omega(m, E)} d\varepsilon,$$

where s, μ, and $\sigma_j^{\text{inv}}(\varepsilon)$ are, respectively, the spin, the reduced mass, and the inverse-reaction cross section for a j-type nucleon of energy ε emitted into a continuum; $\omega(m, E)$ is the density of m-exciton states whose energy is E; and the quantity U has been defined above.

Integrating expression (12) with respect to the energy ε and performing summation in the result over the index j, we find the total probability per unit time for the decay of an m-exciton state via the emission of a neutron or a proton into the continuous spectrum. Specifically, we have

$$\Gamma^{\uparrow}(m, E)/\hbar = \sum_{j=n,p} \int\limits_0^{E-B_j} \lambda_j(m, \varepsilon, E)d\varepsilon. \tag{13}$$

In preequilibrium-decay models, the first order of perturbation theory is used in estimating the intranuclear-transition rate $\Gamma^{\downarrow}(m, E)/\hbar$. This yields [23–25]

$$\Gamma^{\downarrow}(m, E)/\hbar = \frac{2\pi}{\hbar} M^2 \omega_+(m, E), \tag{14}$$

where M^2 is the average square of the two-body transition matrix element and $\omega_+(m, E)$ is the average density of final states accessible in $m \to m + 2$ transitions.

2.1.3. Probability of preequilibrium GDR decay. Preequilibrium GDR decay may be associated with nucleon emission from the $1p1h$ collective doorway state. The probability of such a process is $F(E_{\text{GDR}}) = \Gamma^{\uparrow}_{\text{GDR}} / \left[\Gamma^{\uparrow}_{\text{GDR}} + \Gamma^{\downarrow}_{\text{GDR}}\right]$, where E_{GDR}, $\Gamma^{\uparrow}_{\text{GDR}} = \Gamma^{\uparrow}(2, E_{\text{GDR}})$, and $\Gamma^{\downarrow}_{\text{GDR}} = \Gamma^{\downarrow}(2, E_{\text{GDR}})$ are, respectively, the resonance energy, the emissive GDR width, and the spreading GDR width. The quantities E_{GDR} and $\Gamma^{\downarrow}_{\text{GDR}}$ can be estimated with the aid of semiempirical expressions presented in [6, 37]. The emissive width $\Gamma^{\uparrow}(2, E_{\text{GDR}})$ can be calculated by using expressions (12) and (13).

The quantity $F(E_{\text{GDR}})$ characterizes the probability of the decay of a giant dipole resonance in the region of its maximum. In the region of high energies, the contribution of the initial collective excitation to the state initiated by this excitation decreases in proportion to the ratio $\sigma_{\text{GDR}}(E_\gamma)/\sigma_{\text{GDR}}(E_{\text{GDR}})$. Taking this circumstance into account, we approximate the probability of preequilibrium GDR decay at an arbitrary energy E_γ by the expression

$$F(E_\gamma) = \left[\frac{\Gamma^{\uparrow}_{\text{GDR}}}{\Gamma^{\uparrow}_{\text{GDR}} + \Gamma^{\downarrow}_{\text{GDR}}}\right] \frac{\sigma_{\text{GDR}}(E_\gamma)}{\sigma_{\text{GDR}}(E_{\text{GDR}})}. \tag{15}$$

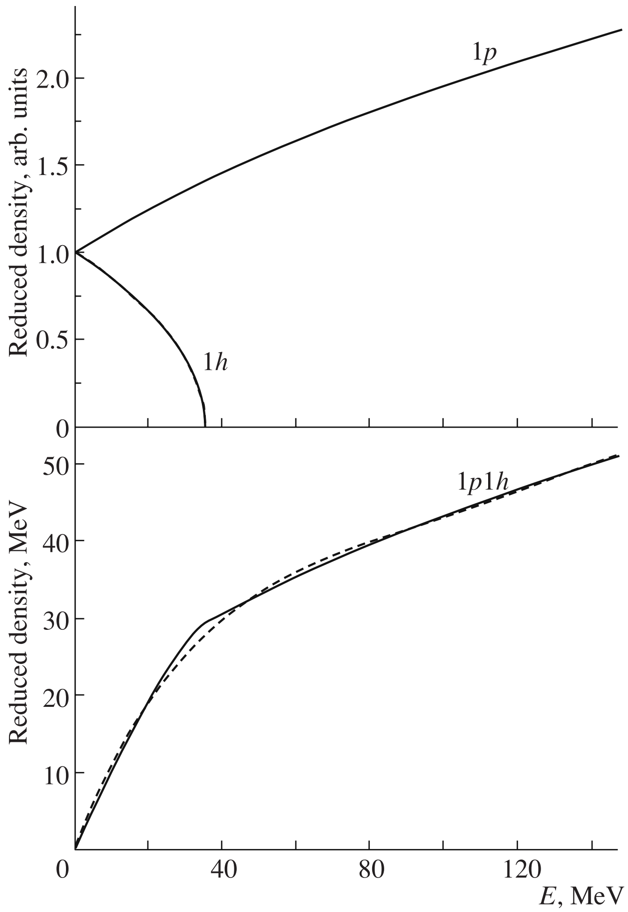

Fig. 1. Reduced Fermi gas densities of $1p$, $1h$, and $1p1h$ states: (solid curves) results of the calculation by formulas (17) and (19) and (dashed curves) approximation by a quartic polynomial (for $1p$ and $1h$ states, these curves merge with the respective solid curves). The nuclear excitation energy is plotted along the abscissa.

2.2. Calculation of Fermi Gas Densities

In the Fermi gas model, the densities of single-particle and single-hole states depend on the excitation energy ϵ and on the type ($j = n, p$) of excited particle or hole:

$$\omega_j(p = 1, h = 0, \epsilon) = c_j \rho(1, 0, \epsilon), \qquad (16)$$
$$\omega_j(p = 0, h = 1, \epsilon) = c_j \rho(0, 1, \epsilon).$$

Here, $c_j = 3N/(2\epsilon_{\rm F})$ for $j = n$ and $c_j = 3Z/(2\epsilon_{\rm F})$ for $j = p$; N and Z are the numbers of, respectively, neutrons and protons in the target nucleus; $\epsilon_{\rm F} \approx 35$ MeV is the Fermi energy; and

$$\rho(1, 0, \epsilon) = \sqrt{\frac{\epsilon_{\rm F} + \epsilon}{\epsilon_{\rm F}}}, \qquad (17)$$
$$\rho(0, 1, \epsilon) = \sqrt{\frac{\epsilon_{\rm F} - \epsilon}{\epsilon_{\rm F}}}$$

are the reduced densities of states for a particle and a hole (they do not depend on the excited-nucleon type or the choice of target nucleus).

The problem of determining the densities $\omega(m, E)$ of ph states reduces to calculating the convolutions of products of the densities in (17) and the delta function $\delta(E - \epsilon_1 - \epsilon_2 - \ldots - \epsilon_m)$ with allowance for the fact that the hole energy cannot exceed the Fermi energy $\epsilon_{\rm F}$. In practice, however, this leads to difficult numerical calculations of multiple integrals with variable limits. As for an analytic solution to the problem at hand, it can be found only for two-exciton states. For example, the expression for the density of *single-particle–single-hole* states has the form

$$\omega_j(p = 1, h = 1, E) = c_j^2 \rho(1, 1, E), \qquad (18)$$

where $j = n, p$; the constants c_n and c_p were defined in (16); and

$$\rho(1, 1, E) = \int\limits_0^{\min(\epsilon_{\rm F}, E)} \rho(0, 1, \epsilon)\rho(1, 0, E - \epsilon) d\epsilon \qquad (19)$$

$$= \begin{cases} \dfrac{2\epsilon_{\rm F} + E}{4\epsilon_{\rm F}}\sqrt{\epsilon_{\rm F}(\epsilon_{\rm F} + E)} \\ - \dfrac{2\epsilon_{\rm F} - E}{4\epsilon_{\rm F}}\sqrt{\epsilon_{\rm F}(\epsilon_{\rm F} - E)} \\ - \dfrac{E^2}{4\epsilon_{\rm F}} \ln\left[\dfrac{\sqrt{\epsilon_{\rm F}} + \sqrt{\epsilon_{\rm F} + E}}{\sqrt{\epsilon_{\rm F}} + \sqrt{\epsilon_{\rm F} - E}}\right] & \text{for } E \le \epsilon_{\rm F}, \\ \dfrac{2\epsilon_{\rm F} + E}{4\epsilon_{\rm F}}\sqrt{\epsilon_{\rm F}(\epsilon_{\rm F} + E)} \\ - \dfrac{E^2}{4\epsilon_{\rm F}} \ln\left[\dfrac{\sqrt{\epsilon_{\rm F}} + \sqrt{\epsilon_{\rm F} + E}}{\sqrt{E}}\right] \\ \text{for } E > \epsilon_{\rm F} \end{cases}$$

is the density of states for a $1p1h$ pair at an excitation energy E.

In order to describe the preequilibrium quasideuteron cascade, which was considered in Subsection 2.1.2, it is necessary to find the densities of only those intermediate states in which the number of particles either is equal to the number of holes or differs from it by unity. These densities can be represented in the form

$$\omega(p, h, E) = \mathcal{C}_m \rho(p, h, E), \qquad (20)$$

$$\omega(p - 1, h, E) = \mathcal{C}_{m-1} \rho(p - 1, h, E),$$

$$\omega(p, h - 1, E) = \mathcal{C}_{m-1} \rho(p, h - 1, E),$$

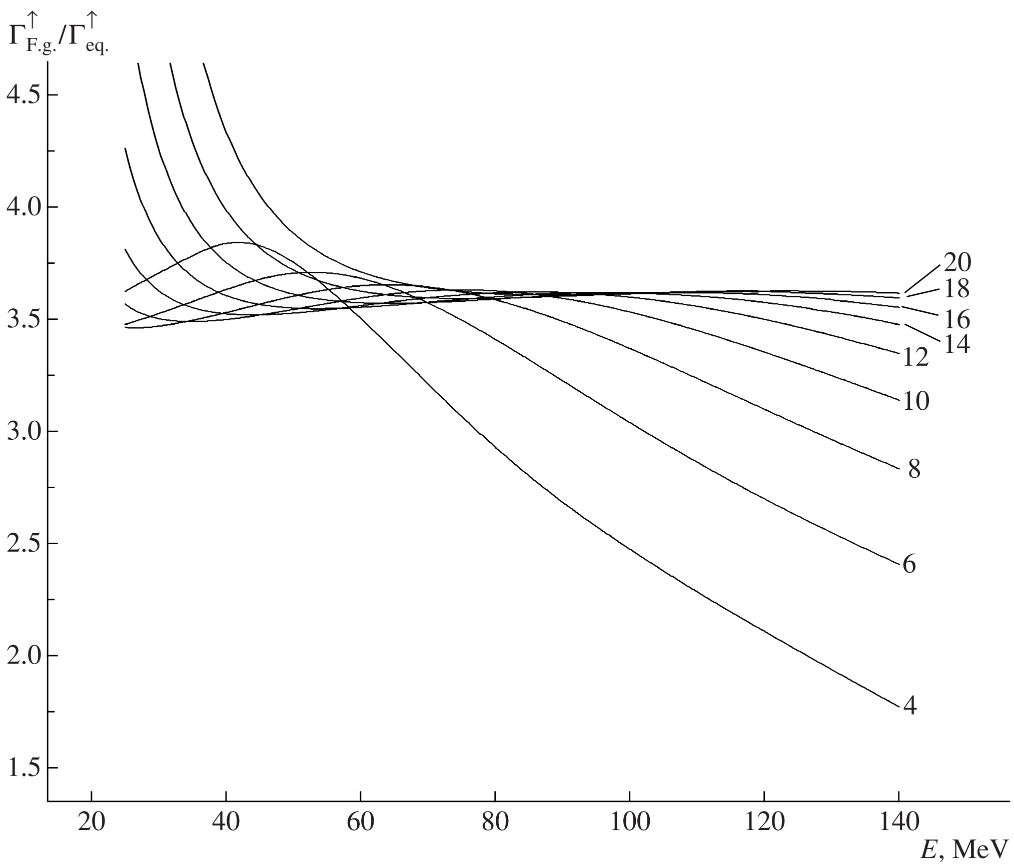

Fig. 2. Ratio of the emissive widths obtained for various m-exciton states of the ^{181}Ta nucleus in the approximation of Fermi gas densities ($\Gamma^{\uparrow}_{\mathrm{F.g.}}(m,E)$) to their counterparts in the approximation of equidistant levels [13] ($\Gamma^{\uparrow}_{\mathrm{eq.}}(m,E)$). The exciton numbers of the states for which the ratios in question were calculated are indicated on the curves. The nuclear excitation energy is plotted along the abscissa.

where

$$\rho(p,h,E) = \int\limits_0^E \int\limits_0^E \ldots \int\limits_0^E \rho(1,1,x_1) \quad (21)$$

$$\times\, \rho(1,1,x_2-x_1) \times \ldots$$

$$\times\, \rho(1,1,x_{m/2-1}-x_{m/2-2})$$

$$\times\, \rho(1,1,E-x_{m/2-1})dx_1dx_2\ldots dx_{m/2-1},$$

$$\rho(p-1,h,E) \quad (22)$$

$$= \int\limits_0^{\min(\epsilon_\mathrm{F},E)} \int\limits_0^E \ldots \int\limits_0^E \rho(0,1,x_1)\rho(1,1,x_2-x_1)$$

$$\times \ldots \times \rho(1,1,x_{m/2-1}-x_{m/2-2})$$

$$\times\, \rho(1,1,E-x_{m/2-1})dx_1dx_2\ldots dx_{m/2-1},$$

$$\rho(p,h-1,E) = \int\limits_0^E \int\limits_0^E \ldots \int\limits_0^E \rho(1,0,x_1) \quad (23)$$

$$\times\, \rho(1,1,x_2-x_1) \times \ldots$$

$$\times\, \rho(1,1,x_{m/2-1}-x_{m/2-2})$$

$$\times\, \rho(1,1,E-x_{m/2-1})dx_1dx_2\ldots dx_{m/2-1}$$

are the reduced densities of states in which we are interested and

$$\mathcal{C}_m = (1.5/\epsilon_\mathrm{F})^m \sum_{i=1}^{m/2-1} \frac{N^{2i}Z^{m-2i}}{(i!(m/2-i)!)^2}, \quad (24)$$

$$\mathcal{C}_{m-1} = (1.5/\epsilon_\mathrm{F})^{m-1} \quad (25)$$

$$\times \sum_{i=1}^{m-2} \frac{N^i Z^{m-i-1}}{[\frac{i}{2}]!(i-[\frac{i}{2}])![\frac{m-i-1}{2}]!(m-i-1-[\frac{m-i-1}{2}])!}$$

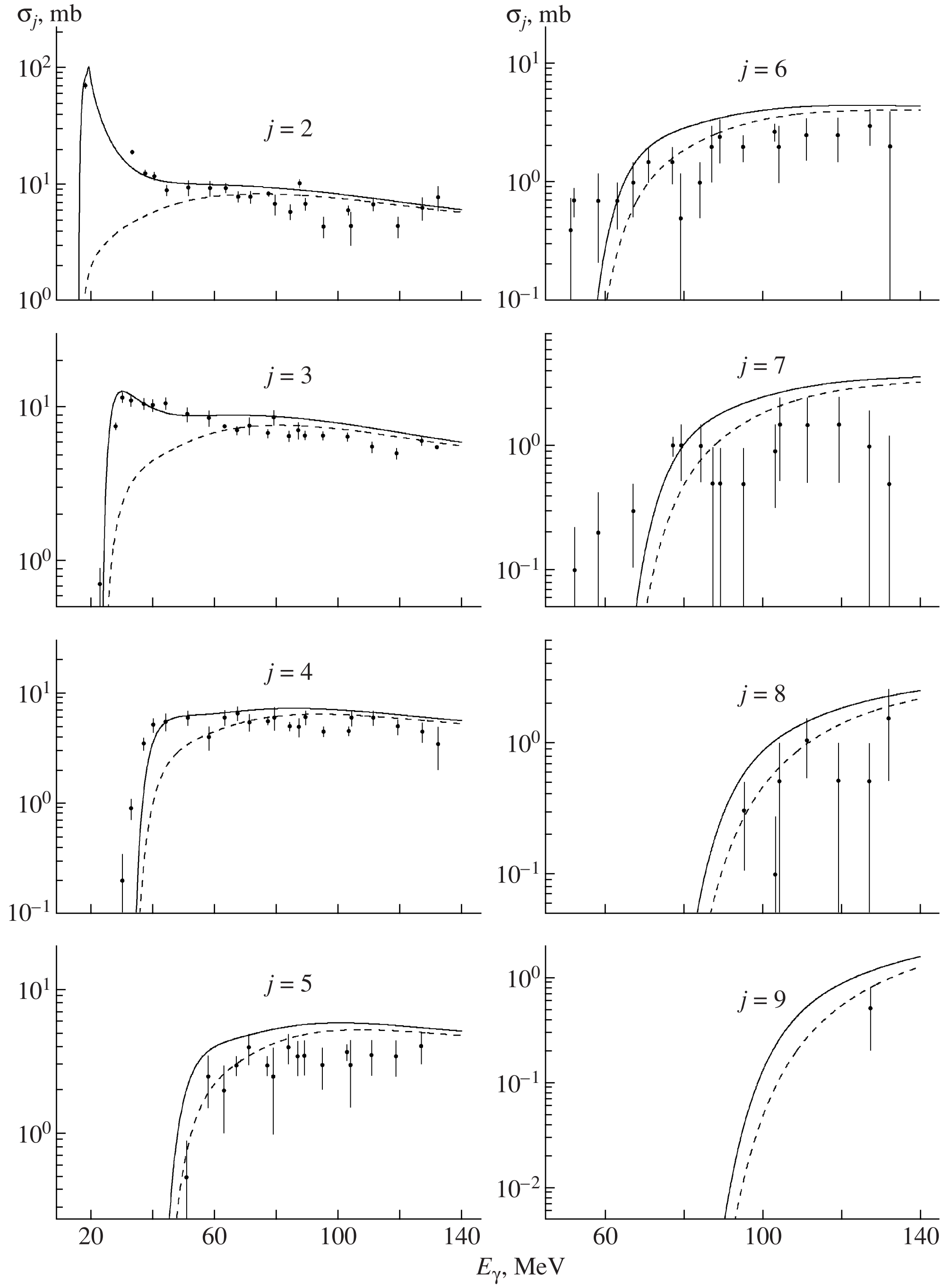

Fig. 3. Cross sections $\sigma_j(E_\gamma)$ for photonucleon reactions proceeding on tin nuclei and involving the emission of $j, j+1, \ldots$ neutrons plus an arbitrary number of charged particles: (points with error bars) experimental data for a target from tin of natural isotopic composition [35], (solid curves) cross sections calculated for the ^{119}Sn nucleus, and (dashed curves) quasideuteron components of the theoretical cross sections.

are normalization constants that take into account the presence of a neutron and a proton component in m-exciton states. By $[x]$, we mean the integral part of x; also, $p = h = m/2$ and $m = 4, 6, 8, \ldots$.

The integrals in (21)–(23) can readily be calculated upon approximating the reduced densities $\rho(1,0,\epsilon)$, $\rho(0,1,\epsilon)$, and $\rho(1,1,\epsilon)$ by polynomials. Figure 1 displays the results obtained for the case where these functions are approximated by expressions (17) and (19) (solid curves) and for the case

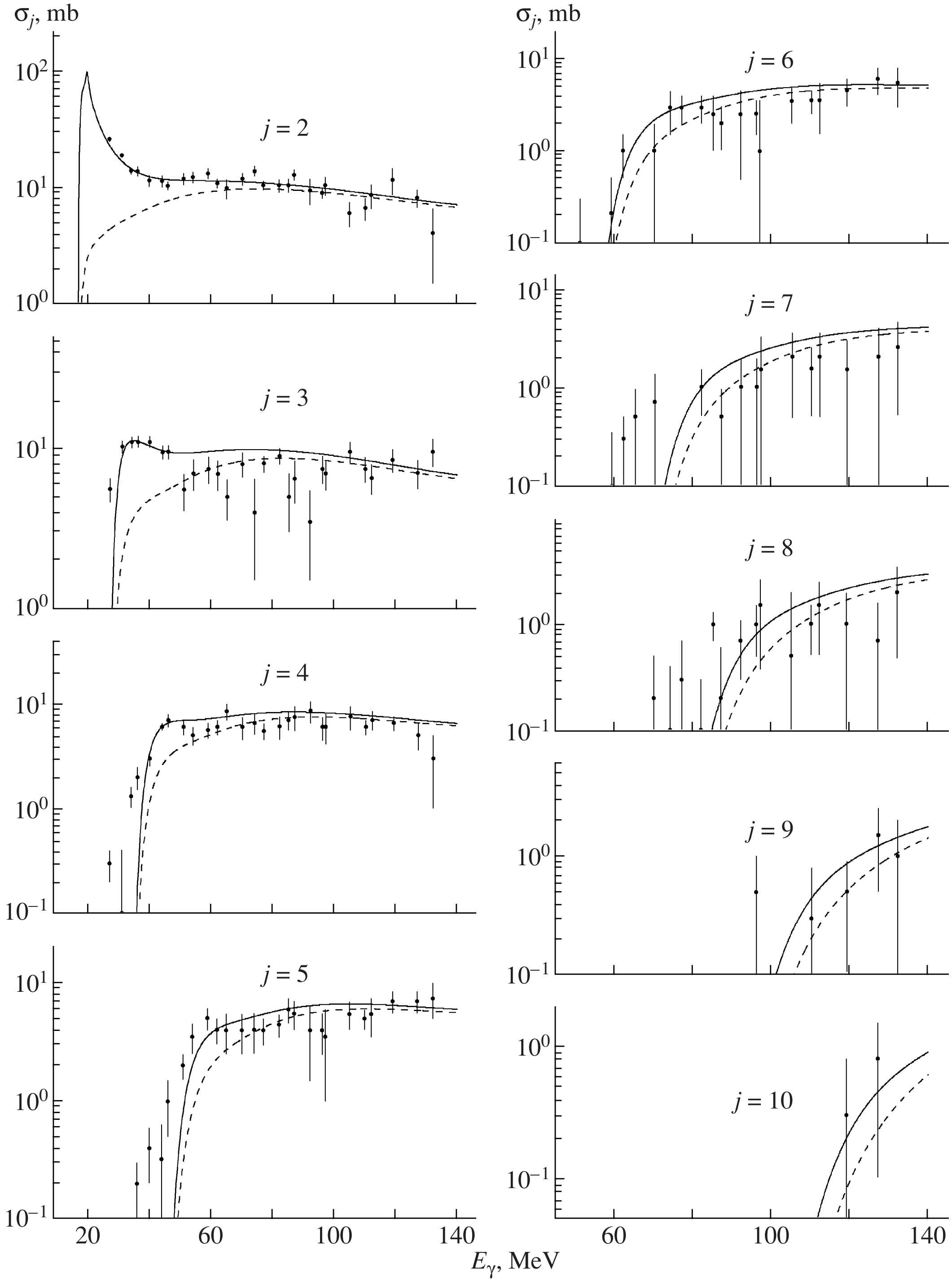

Fig. 4. Calculated (for ^{140}Ce) and experimental [35] (for cerium of natural isotopic composition) photonucleon cross sections $\sigma_j(E_\gamma)$. The notation is identical to that in Fig. 3.

where they are approximated by quartic polynomials (dashed curves). The attained degree of approximation seems quite sufficient, the more so as the Fermi gas densities themselves are an approximation to realistic densities of ph states.

The average density of final states accessible in $m \to m+2$ transitions is given by

$$\omega_+(m, E) = \mathcal{N}_m \left[\int\limits_0^E \rho(2,1,\epsilon)\rho(1,0,\epsilon) \right. \qquad (26)$$

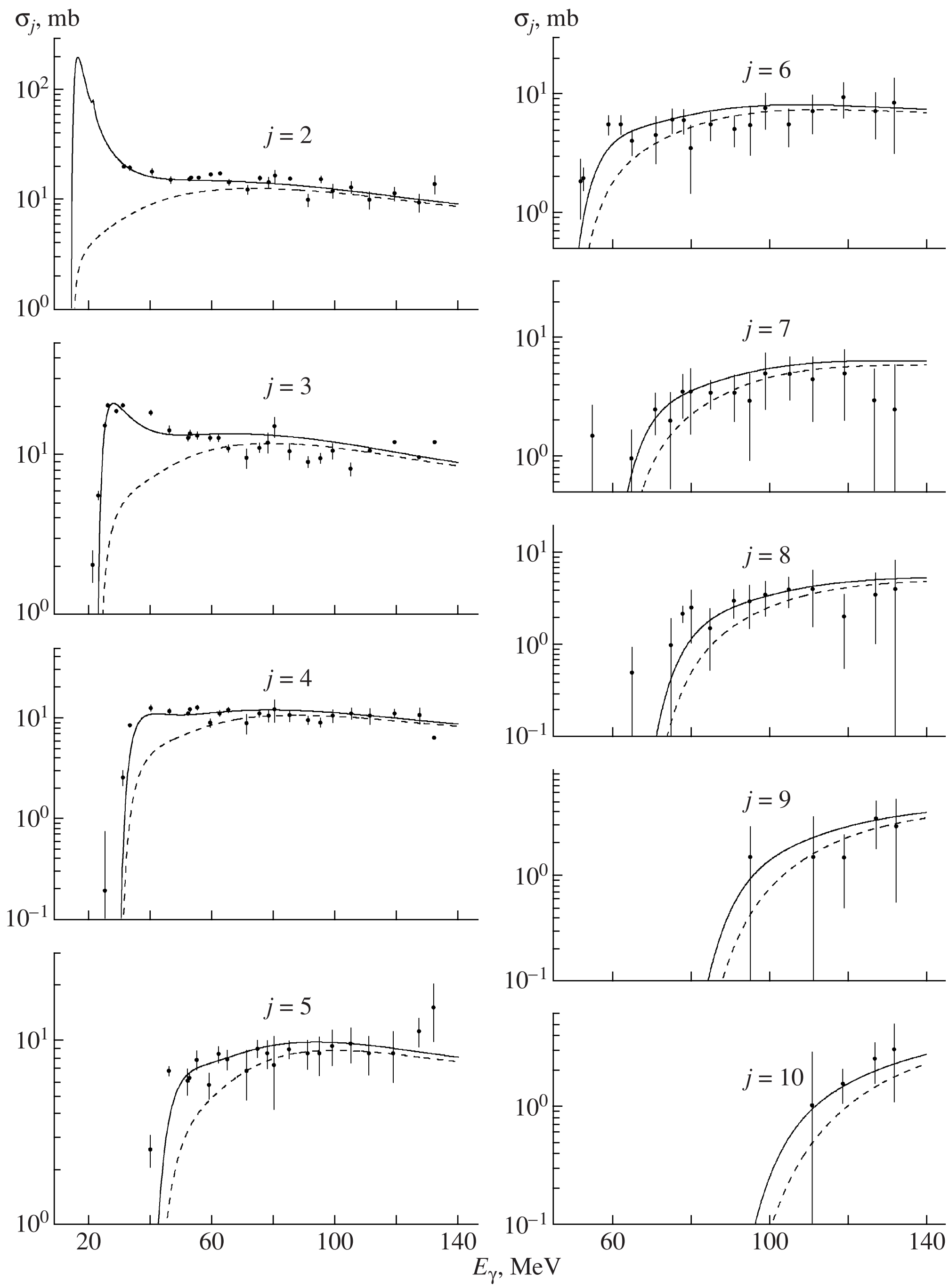

Fig. 5. Calculated (for ^{181}Ta) and experimental [35] (for tantalum of natural isotopic composition) photonucleon cross sections $\sigma_j(E_\gamma)$. The notation is identical to that in Fig. 3.

$$\times \rho(p-1,h,E-\epsilon)d\epsilon + \int\limits_0^{\min(\epsilon_{\rm F},E)} \rho(1,2,\epsilon)$$

$$\times \rho(0,1,\epsilon)\rho(p,h-1,E-\epsilon)d\epsilon \Bigg] \Bigg/ \rho(p,h,E),$$

where

$$\mathcal{N}_m = \frac{m}{8}\left(\frac{3A}{2\epsilon_{\rm F}}\right)^3\left(1-\frac{NZ}{A^2}\right) \qquad (27)$$

is a normalization coefficient that takes into account the neutron–proton composition of decaying m-exciton states, $p = h = m/2$, and $m = 2, 4, 6, \ldots$

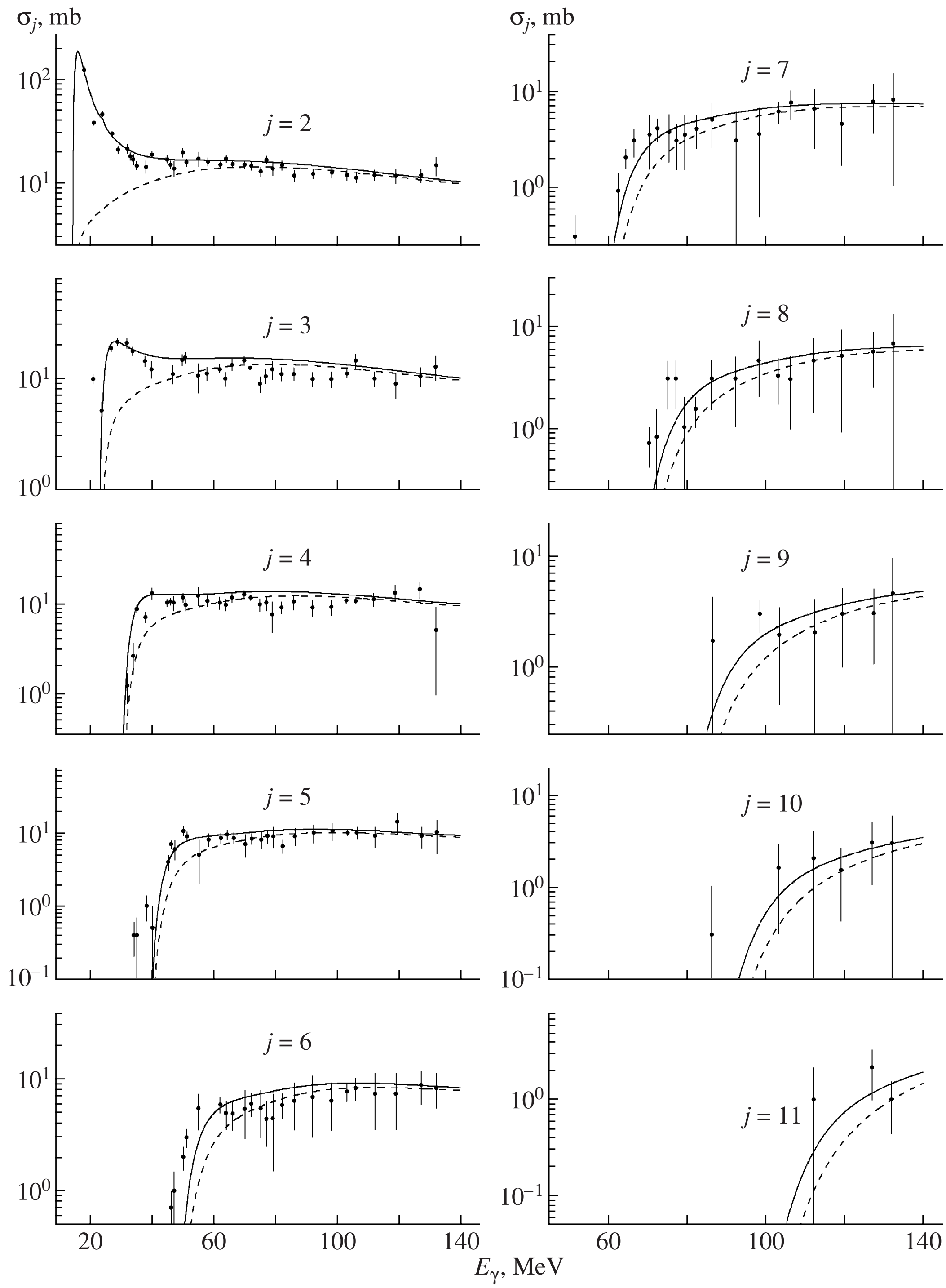

Fig. 6. Calculated (for ^{208}Pb) and experimental [35] (for lead of natural isotopic composition) photonucleon cross sections $\sigma_j(E_\gamma)$. The notation is identical to that in Fig. 3.

Figure 2 displays the ratios $\Gamma^{\uparrow}_{\text{F.g.}}(m, E)/\Gamma^{\uparrow}_{\text{eq}}(m, E)$ of the emissive widths calculated for various m-exciton states of the ^{181}Ta nucleus with the aid of Fermi gas densities to their counterparts calculated with the aid of equidistant-level densities corrected for the Pauli exclusion principle and for a finite potential-well depth [13]. From this figure, one can see that a transition to Fermi gas densities leads to a substantial increase in the contribution of preequilibrium nucleon emission. As was indicated in the Introduction, this is due to an increase in the fraction of high-energy particles at each stage of the preequilibrium cascade.

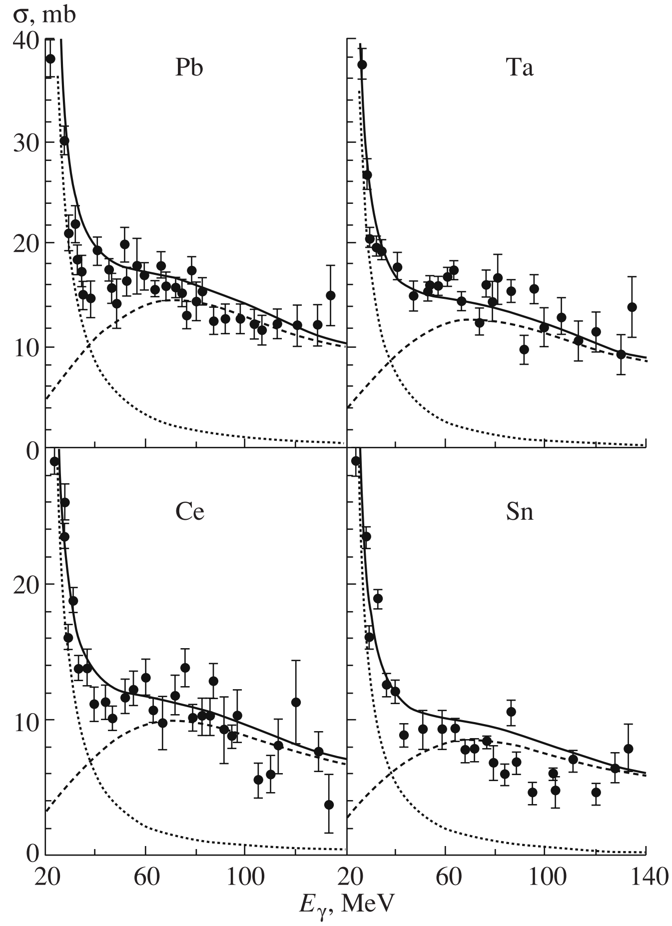

Fig. 7. Cross sections for photoabsorption on Pb, Ta, Ce, and Sn nuclei from [3]. The points with error bars stand for experimental data from [35]. The solid, dashed, and dotted curves represent, respectively the total theoretical cross sections for photoabsorption, the calculated quasideuteron components of photoabsorption from [3], and the contribution of GDR tails to the theoretical cross section [35].

3. APPLICATION TO DESCRIBING PHOTONUCLEON REACTIONS ON ^{119}Sn, ^{140}Ce, ^{181}Ta, AND ^{208}Pb

3.1. Details of the Computational Procedure

In order to describe cross sections for GDR excitation ($\sigma_{\rm GDR}(E_\gamma)$), we employed the semimicroscopic model proposed in [6]. The quadrupole-deformation parameter β, which is the only free parameter in the model, was estimated on the basis of data on static quadrupole moments of nuclei [7]. This yielded β values of about 0.0, 0.02, 0.26, and 0.0 for the ^{119}Sn, ^{140}Ce, ^{181}Ta, and ^{208}Pb nuclei, respectively. The quasideuteron component of the photoabsorption cross section ($\sigma_{\rm QD}(E_\gamma)$) was calculated on the basis of the model proposed in [1–3], the model parameters being set to the values from [3]. The inverse-reaction cross sections $\sigma_p^{\rm inv}(\varepsilon)$ and $\sigma_n^{\rm inv}(\varepsilon)$ [see Eq. (12)] were calculated by using approximate expressions from the monograph of Barashenkov and Toneev [38].

The level-density parameter a, the average number $\bar{m}$ of excitons in the state of thermal equilibrium, and the average square M^2 of the transition matrix element are intrinsic parameters of the model being considered. We employed the usual choice of value for the level-density parameter: $a = g\pi^2/6$, where $g \approx A/13$ is the density of single-particle states in the model of equidistant levels. The parameter $\bar{m} = \bar{m}(E)$, which appears in Eqs. (9) and (10), was determined from the requirement that, in the state of thermal equilibrium, the average energy per exciton be 3/2 of the temperature of the nucleus at a given excitation energy; that is,

$$\frac{E}{\bar{m}} = \frac{3}{2}\Theta = \frac{3\sqrt{E/a}}{2(1-2/\sqrt{aE})}. \tag{28}$$

The average square of the transition matrix element, $M^2 = M^2(E)$, was approximated by the expression

$$M^2(E) = M^2(E_{\rm GDR})\frac{E_{\rm GDR}}{E}, \tag{29}$$

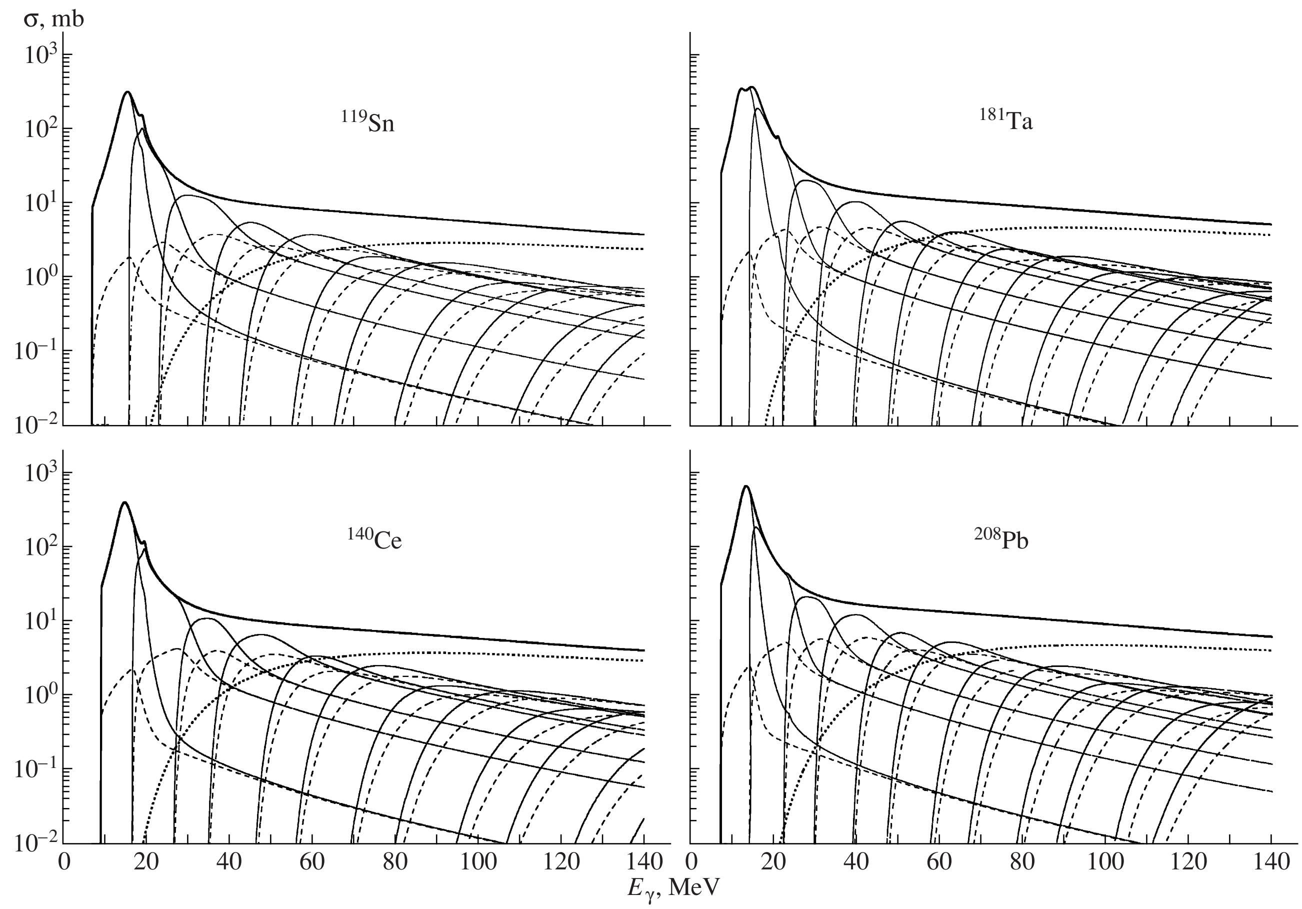

Fig. 8. Calculated photonucleon cross sections for ^{119}Sn, ^{140}Ce, ^{181}Ta, and ^{208}Pb nuclei: (thin solid curves) cross sections for the (γ, kn), $k = 1, 2, \ldots$, reactions; (dashed curves) contribution of the quasideuteron component to these cross sections; (thick solid curves) total photoneutron cross section $\sum_{k=1}^{\infty} \sigma(\gamma, kn; E_\gamma)$; and (dotted curves) total cross section for processes involving proton emission, $\sum_{l=0}^{\infty} \sigma(\gamma, 1pln; E_\gamma)$.

where $E_{\rm GDR}$ is the GDR energy and the factor E^{-1} takes into account the empirical energy dependence of the square of the matrix element [11].

We determined the constant $M^2(E_{\rm GDR})$ from relation (14), in which we substituted the following estimate from [6] [Eqs. (65) and (53) there] for the spreading GDR width: $\Gamma^{\downarrow}_{\rm GDR} = \Gamma^{\downarrow}(2, E_{\rm GDR})$.

Our computations involved evaluating the cross sections for the (γ, kn), $k = 1$–12, and $(\gamma, 1pln)$, $l = 0$–12, reactions on ^{119}Sn, ^{140}Ce, ^{181}Ta, and ^{208}Pb nuclei in the low-energy range $7 \le E_\gamma \le 140$ MeV with a step of 0.1 MeV.

3.2. Discussion of the Results

The basic results of our calculations are displayed in Figs. 3–9. As was indicated above (see Introduction), a comparison of experimental and theoretical results on partial cross sections for reactions accompanied by the emission of various numbers of nucleons into the continuous spectrum provides the best test of preequilibrium calculations. A vast body of data for such an analysis was obtained by a group of experimentalists from Saclay. Upon separating the neutron yields of different multiplicity, they were able to measure the total cross sections $\sigma_j(E_\gamma)$, $2 \le j \le 11$, for reactions occurring on natural mixtures of tin, cerium, tantalum, and lead isotopes in the energy range 25–132 MeV and involving the emission of j or more neutrons plus any number of charged particles into a continuum [35]. Within the model being considered, these cross sections can be expressed in terms of the cross sections $\sigma(\gamma, kn; E_\gamma)$ and $\sigma(\gamma, 1pln; E_\gamma)$ introduced in Subsection 2.1 [see Eqs. (2) and (3)]:

$$\sigma_j(E_\gamma) = \sum_{k=j}^{\infty} \left(\sigma(\gamma, kn; E_\gamma) + \sigma(\gamma, 1pkn; E_\gamma) \right). \quad (30)$$

Figures 3–6 give the theoretical cross sections

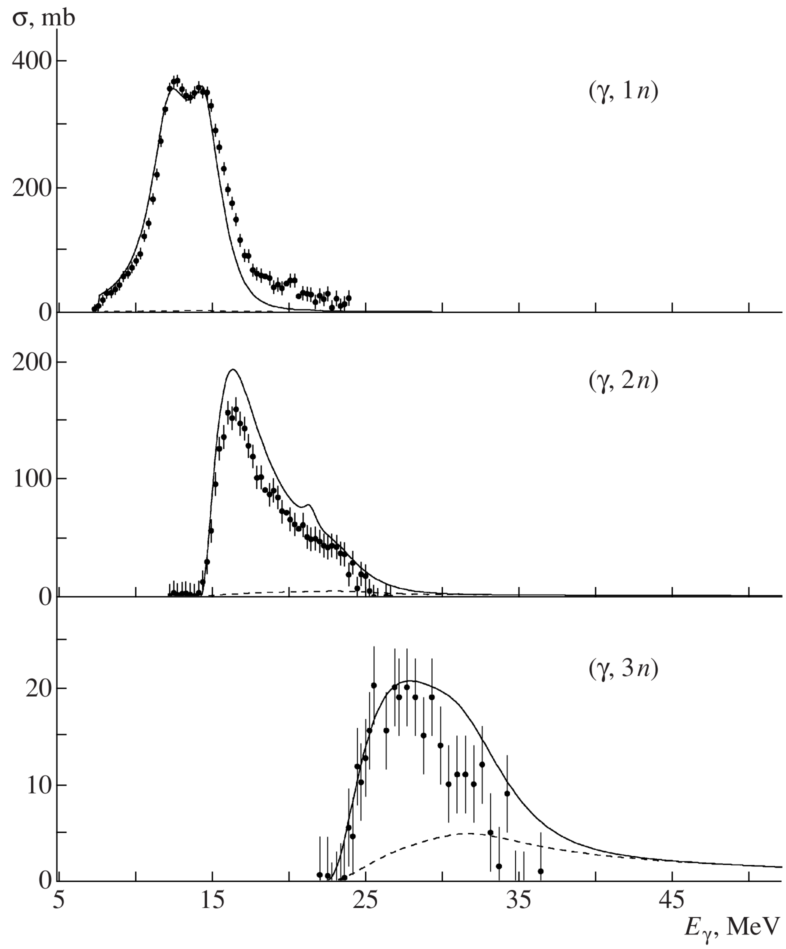

Fig. 9. Calculated and experimental photoneutron cross sections for the $(\gamma, 1n)$, $(\gamma, 2n)$, and $(\gamma, 3n)$ reactions on ^{181}Ta nuclei: (points with error bars) experimental data from [39, 40], (solid curves) calculated cross sections, and (dashed curves) quasideuteron components of theoretical cross sections.

$\sigma_j(E_\gamma)$ (solid curves) calculated for the ^{119}Sn, ^{140}Ce, ^{181}Ta, and ^{208}Pb nuclei, whose mass numbers are the closest to the average mass numbers of tin, cerium, tantalum, and lead targets of natural isotopic composition. They are compared with experimental data (points with statistical-error bars) obtained in [35]. The dashed curves represent the quasideuteron components of the theoretical cross sections. From Figs. 3–6, one can see that, by and large, the results of the calculations agree fairly well with the experimental data in question. The discrepancy between the theoretical and experimental results in threshold regions is due primarily to the fact that targets of natural isotopic composition contain isotopes characterized by neutron separation energies lower than those used in the calculations, as well as to a finite experimental energy resolution.

For tin, all of the calculated cross sections $\sigma_j(E_\gamma)$ are systematically in excess of their experimental counterparts in the energy region $E_\gamma \gtrsim 70$ MeV (see Fig. 3). The origin of this excess is clarified by Fig. 7, which was borrowed from [3] and in which theoretical and experimental [35] cross sections for photoabsorption on Pb, Ta, Ce, and Sn nuclei are compared in the energy range $20 \leq E_\gamma \leq 140$ MeV. From this figure, one can see that, while, for Pb, Ta, and Ce nuclei, the agreement between the theoretical and experimental results is more or less satisfactory, for Sn, the theoretical photoabsorption curve lies substantially higher (owing primarily to the quasideuteron component) than respective experimental data in the range $70 \lesssim E_\gamma \lesssim 120$ MeV. Thus, the observed disagreement between the theory and experiment is due either to systematic experimental errors or to a not quite correct description of photoabsorption at high energies E_γ on medium-mass nuclei within the quasideuteron model [1–3].

From Figs. 3–6, one can see that the GDR component of photonucleon reactions is dominant at low excitation energies of the nucleus being considered

($E \lesssim 30$ MeV) and also plays a significant role in the region of high energies in describing cross sections for reactions accompanied by the emission of a large number of neutrons. The last circumstance is explained by a sharp decrease in the population of residual nuclei in the lower (in A) part of the quasideuteron cascade because of the emission of a preequilibrium nucleon carrying away a significant amount of energy from the nucleus.

One can draw similar conclusions from the data in Fig. 8, which shows the cross sections for (γ, kn), $k = 1, 2, \ldots$, reactions (thin solid curves); their quasideuteron components (dashed curves); the total photoneutron cross section $\sum_{k=1}^{\infty} \sigma(\gamma, kn; E_\gamma)$ (thick solid curves); and the total cross section for processes involving the emission of a proton, $\sum_{l=0}^{\infty} \sigma(\gamma, 1pln; E_\gamma)$ (dotted curves). According to the data in Fig. 8, the ratio of the cross section for processes involving proton emission to the cross section for processes in which there is no proton emission grows from about 0.1 at $E_\gamma = 40$ MeV to about 0.7 at $E_\gamma = 140$ MeV.

In Fig. 9, the calculated cross sections for the $(\gamma, 1n)$, $(\gamma, 2n)$, and $(\gamma, 3n)$ reactions on ^{181}Ta nuclei (solid curves) are contrasted against their experimental counterparts from [39, 40] (points with error bars). The dashed curves represent the contribution of the quasideuteron component to the theoretical cross sections. With allowance for the systematic errors of the measurements in a quasimonochromatic photon beam, the resulting agreement between theoretical and experimental cross-section values seems quite satisfactory. From Fig. 9, it can be seen that the cross sections being considered are determined primarily by processes caused by GDR decay. Quasideuteron photoabsorption plays a significant role only in the formation of the cross section $\sigma(\gamma, 3n)$.

4. CONCLUSIONS

The calculations performed above have revealed that a combination of the evaporation model with the exciton model that is based on Fermi gas densities makes it possible to obtain quite a satisfactory description of partial photonucleon cross sections for medium-mass and heavy nuclei in the energy region below the pion-production threshold.

The proposed model possesses a high predictive power since its parameters either are chosen in a standard way or are determined from semiempirical relations (as is done in normalizing the mean square of the matrix element, M^2).

A transition from the densities of equidistant levels to more realistic Fermi gas densities makes it possible to take into account the effect of the energy dependence of single-particle and single-hole densities on the rate of emissive and intranuclear processes. This circumstance is of paramount importance in describing photonucleon reactions in the high-energy region, where the quasideuteron photoabsorption mechanism is dominant. In the case of employing Fermi gas densities, primary preequilibrium particle emission begins to play a much more important role, determining, together with evaporation processes, the quasideuteron component of photonucleon reactions.

ACKNOWLEDGMENTS

We are deeply indebted to S.S. Belyshev for his general assistance in preparing the manuscript for publication.

This work was supported by a grant (no. 1619.2003.2) from the President of the Russian Federation for support of leading scientific schools.

REFERENCES

1. J. S. Levinger, Phys. Rev. **84**, 43 (1951).
2. J. S. Levinger, Phys. Lett. B **82**, 181 (1979).
3. M. B. Chadwick et al., Phys. Rev. C **44**, 814 (1991).
4. B. S. Ishkhanov and V. N. Orlin, Yad. Fiz. **66**, 1269 (2003) [Phys. At. Nucl. **66**, 1229 (2003)].
5. B. S. Ishkhanov and V. N. Orlin, Yad. Fiz. **67**, 614 (2004) [Phys. At. Nucl. **67**, 595 (2004)].
6. B. S. Ishkhanov and V. N. Orlin, Fiz. Élem. Chastits At. Yadra **38**, 460 (2007) [Phys. Part. Nucl. **38**, 232 (2007)].
7. N. Stone, *Table of New Nuclear Moments*, Preprint, 1997 (a revision of the *Table of Nuclear Moments* by P. Raghavan, At. Data Nucl. Tables **42**, 189 (1989)); http://www.nndc.bnl.gov/nndc/stone-moments.
8. J. R. Wu and C. C. Chang, Phys. Rev. C **16**, 1812 (1977).
9. M. Blann et al., Phys. Rev. C **28**, 2286 (1983).
10. C. K. Cline and M. Blann, Nucl. Phys. A **172**, 225 (1971).
11. C. K. Cline, Nucl. Phys. A **210**, 590 (1973).
12. E. Gadioli, E. Gadioli Erba, and P. G. Sona, Nucl. Phys. A **217**, 589 (1973).
13. J. Dobes and E. Beták, Nucl. Phys. A **272**, 353 (1976).
14. M. Blann, Phys. Rev. Lett. **27**, 337 (1971).
15. M. Blann, Phys. Rev. Lett. **28**, 757 (1972).
16. M. Blann and H. K. Vonach, Phys. Rev. C **28**, 1475 (1983).
17. M. B. Chadwick and P. G. Young, Acta Phys. Slov. **45**, 633 (1995).
18. H. Feshbach, A. Kerman, and S. Koonin, Ann. Phys. (N.Y.) **125**, 429 (1980).
19. J. J. Griffin, Phys. Rev. Lett. **17**, 478 (1966).
20. T. Tamura, T. Udagawa, and H. Lenske, Phys. Rev. C **26**, 379 (1982).

21. H. Nishioka et al., Ann. Phys. (N.Y.) **172**, 67 (1986).
22. H. Nishioka, H. A. Weidenmüller, and S. Yoshida, Ann. Phys. (N.Y.) **183**, 166 (1988).
23. J. M. Akkermans and A. J. Koning, Phys. Lett. B **234**, 417 (1990).
24. A. J. Koning and J. M. Akkermans, Ann. Phys. (N.Y.) **208**, 216 (1991).
25. A. J. Koning and M. B. Chadwick, Phys. Rev. C **56**, 970 (1997).
26. C. Kalbach, J. Phys. G **21**, 1519 (1995).
27. A. J. Koning and M. C. Duijvestijn, Nucl. Phys. A **744**, 15 (2004).
28. J. Bisplinghoff, Phys. Rev. C **33**, 1569 (1986).
29. M. Blann, Phys. Rev. C **54**, 1341 (1996).
30. M. Blann and M. B. Chadwick, Phys. Rev. C **57**, 233 (1998).
31. C. A. Soares Pompeia and B. V. Carlson, Phys. Rev. C **74**, 054609 (2006).
32. T. E. O. Ericson, Adv. Phys. **9**, 425 (1960).
33. F. C. Williams, Nucl. Phys. A **166**, 231 (1971).
34. H. Vonach et al., Phys. Rev. C **50**, 1952 (1994).
35. A. Lepretre et al., Nucl. Phys. A **367**, 237 (1981).
36. J. M. Blatt and V. F. Weisskopf, *Theoretical Nuclear Physics* (Wiley, New York, 1952; Inostrannaya Literatura, Moscow, 1954).
37. B. S. Ishkhanov and V. N. Orlin, Yad. Fiz. **66**, 688 (2003) [Phys. At. Nucl. **66**, 659 (2003)].
38. V. S. Barashenkov and V. D. Toneev, *Interactions of High-Energy Particles and Nuclei with Nuclei* (Atomizdat, Moscow, 1972) [in Russian].
39. R. Bergere, H. Beil, and V. Veyssiere, Nucl. Phys. A **121**, 463 (1968).
40. R. L. Bramblett et al., Phys. Rev. **133**, B869 (1964).

Translated by A. Isaakyan